Speciation of Cu and Zn in bottom ash from solid waste incineration studied by XAS, XRD, and geochemical modelling

Charlotta Tiberg [a,*], Carin Sjöstedt [b], Karin Karlfeldt Fedje [c,d]

[a] *Swedish Geotechnical Institute, SE-581 93 Linköping, Sweden*
[b] *Department of Soil and Environment, Swedish University of Agricultural Sciences, SE-750 07 Uppsala, Sweden*
[c] *Recovery and Management, Renova AB, Box 156, SE-401 22 Gothenburg, Sweden*
[d] *Department of Architecture and Civil Engineering, Division of Water Environment Technology, Chalmers University of Technology, SE-412 96 Gothenburg, Sweden*

ARTICLE INFO

ABSTRACT

Millions of tons of bottom ash (BA) is generated from incineration of industrial and municipal solid waste each year within EU. The magnitude of leaching of metals like Cu and Zn is critical for hazard and risk assessment of these ashes. Although speciation of metals is a key factor to understand and predict metal leaching, speciation of Cu and Zn in BA is not well known. In this study six metal separated and carbonized BA were investigated by a combination of X-ray absorption spectroscopy, X-ray diffraction, leaching/extraction tests, and geochemical modelling. Five of the BA were from grate boilers and one from a fluidized bed incinerator. The aims were to identify similarities in Cu and Zn speciation and to identify main species. The combination of several techniques was necessary to draw conclusions about speciation and displayed coherent results. A similar speciation of Cu and Zn was indicated in the five studied grate boiler ashes although the proportions between species may vary. Copper(II) oxide and Cu metal were the main Cu species in all BA. Zinc(II) oxide and willemite (Zn_2SiO_4) were identified in grate boiler ashes. The fluidized bed ash contained Zn-Si-minerals and possibly franklinite or gahnite, while the Zn(II) oxide content was low, if any. The results have implications for classification and risk assessment of MIBA.

© 2020 The Authors. Published by Elsevier Ltd. This is an open access article under the CC BY license (http://creativecommons.org/licenses/by/4.0/).

1. Introduction

Incineration with energy recovery is a commonly used management method for industrial and municipal solid waste. In Sweden only, approximately 1 million tons of bottom ash is generated from waste incineration annually (Avfall Sverige, 2005). In EU, Norway, and Switzerland together the annual generation is almost 18 million tons (Blasenbauer et al., 2020). With the most common technique, mass burn combustion, bottom ash (BA) accounts for ~80% of the total ash amount, while the remaining ~20% is fly ash. Fly ash generally contains larger amounts of metals and chlorides compared to bottom ash and is therefore frequently regarded as hazardous waste, which limits its utilization. In contrast, the BA can after treatment be used for different construction purposes. The

treatment procedure involves sorting out metal pieces followed by natural weathering ("aging") to make the bottom ash more stable to metal leaching by means of e.g. carbonation. During the carbonation process, CO_2 is absorbed by alkaline compounds in the ash, such as $Ca(OH)_2$, and carbonates, mainly $CaCO_3$, are formed (Freyssinet et al., 2002). The metal content does not decrease through this process, but leaching is generally reduced as the pH decreases to slightly alkaline and metals can transform into less soluble species (Arickx et al., 2006). Bottom ashes that have gone through this process are hereafter referred to as MIBA, *mineral fraction of incinerator bottom ash*, a term suggested to distinguish unprocessed BA from processed BA (Blasenbauer et al., 2020).

Statistics from, among others, Eurostat (the statistical office of the European Union) and CEWEP (Confederation of European Waste-to-Energy Plants) on the utilization of stabilized and aged bottom ash was recently compiled (Blasenbauer et al., 2020; Dou et al., 2017). In some European countries like Denmark and the Netherlands MIBA is used as a complement to sand and gravel in e.g. road constructions and embankments, while in other countries it is primarily used within landfills due to concerns of metal leaching from the material (Blasenbauer et al., 2020; Dou et al., 2017).

The latter is the common practice in e.g. Lithuania, Norway, and Sweden. One important factor influencing utilization of MIBA is classification as hazardous or non-hazardous waste and especially the hazardous property ecotoxicity (HP 14) is of high concern (European Parliament and Council, 2008). However, to what extent leaching from and presence of metals in MIBA poses a threat to the environment and how this should be evaluated is still not entirely clear. Identification of metal species in the ash and deeper understanding of the mechanisms regulating metal solubility will narrow this knowledge gap. The speciation of elements in (MI)BA depends on the composition of the incinerated waste, the combustion method and treatment of the ash. The dominating minerals are usually the same and include silicate minerals, e.g. SiO_2 and feldspars, Al and Fe oxides/hydroxides and $CaO/CaCO_3$ (Bayuseno, 2006; Kowalski et al., 2017; Stiernström et al., 2016). Speciation of minor and trace elements in MIBA is less known as their lower concentration complicate speciation studies, but of high importance since these elements are often crucial for the classification (European Parliament and Council, 2008). In addition, prediction of potential leachability will be more accurate with better knowledge about the speciation. Two such elements are Cu and Zn. Different analytical methods, but most commonly X-ray diffraction (XRD), have been used in attempts to identify Cu and Zn species. Several dissimilar Cu and Zn species have been suggested to be present in MIBA, including various mineral phases (e.g. oxides, hydroxides), adsorption to Fe/Al-hydroxides and metallic Cu and Zn (Table 1). However, due to methodological limitations, one analytical method alone often cannot unambiguously determine speciation of minor and trace elements in a matrix as complicated as (MI)BA and few studies have used a combination of several methods to identify species in (MI)BA (Table 1). For example, XRD can only identify crystalline minerals comprising at least a few percent of the matrix, while geochemical modelling suggests solubility controlling species which are not necessarily the same as the main forms. A method with large potential that has not been abundantly used on MIBA is X-ray absorption spectroscopy (XAS) measurements (*X-ray absorption near edge structure,* XANES, or *extended X-ray absorption fine structure,* EXAFS) (Table 1). This method can give direct information on the predominating species of a specific metal and includes negligible need of sample preparation as well as non-destroyable analysis. In addition, non-crystalline elements can be identified and, compared to XRD, species can be identified in lower concentrations, why this method is especially suitable for minor and trace elements. On the contrary, it requires expensive and advanced equipment and the data evaluation may be complicated for complex matrices like MIBA.

In the present study, speciation of Cu and Zn in six MIBA was investigated by a combination of analytical methods including EXAFS spectroscopy, XRD, and pH-dependent leaching evaluated by geochemical modelling. The aims were to: 1) Identify similarities in Cu and Zn speciation between the studied MIBA. 2) Identify main Cu and Zn species in the ashes. This knowledge will contribute to better predictions of potential leaching from the ashes and improve the basis for hazard and risk assessments of metal sorted and carbonated bottom ash i.e. MIBA. The study also contributes with experience on the possibilities to identify Cu and Zn species in (MI)BA by EXAFS spectroscopy in combination with the other techniques.

2. Materials and methods

2.1. Bottom ashes

The MIBA samples used in this project were collected at six different Swedish Waste-to-Energy plants (A-F), whereof five are grate fired boilers (G) and one is bubbling fluidized bed (BFB, sample denoted FB-D), Table 2. Fluidized bed combustion is less common compared to gate fired boilers but still frequently used. The main difference between BA from these techniques is the higher presence of silicates in the FB ash, which is due to sand addition to the bed to receive more even combustion. All plants delivering ash to this study are large, modern, facilities and the fuel used is household and industrial waste. All samples, except sample A, were mechanically metal separated and naturally carbonated outdoors for at least 4 months. Sample G-A was manually metal separated and carbonated in the laboratory until the pH reached 10. All chemical analysis and leaching/extraction tests of MIBA was performed at laboratories quality accredited pursuant to ISO 17025.

2.2. Characterization and XRD analysis

Elemental concentrations in the original bottom ash samples were analyzed with ICP-AES after microwave assisted digestion with a hydrofluoric (HF), nitric (HNO_3), and hydrochloric (HCl) acid mixture according to SS-EN-13656. The contents of organic (TOC) and inorganic carbon (TIC) were analyzed using SS-EN 13137, while pH was measured according to SS-EN 15933. For sample C and D the pH was only measured in L/S 10 leachates (SS-EN-12457-2). Analyzes were performed in duplicate or triplicate. XRD measurements were performed on ground samples from 5° to 65° with STOE ⊙/⊙- Diffractometer and a CuK$_\alpha$ x-ray tube.

2.3. Extended X-ray absorption fine structure

EXAFS measurements were performed at Stanford Synchrotron Radiation Lightsource, SSRL (Table 2). Samples G-A, G-B, G-C and FB-D were crushed and sieved to <0.25 mm before analysis. G-E and G-F were ground in a ball mill to very fine particle size. All samples were mounted in an Al sample holder, sealed with Kapton® tape.

All Fe and Cu XAS spectra as well as the Zn spectra for MIBA G-C, FB-D, G–E and G-F were collected at the wiggler beamline 4-1, equipped with a liquid N_2-cooled Si(2 2 0) double crystal monochromator. Measurements were conducted at liquid N_2-temperature (80 K) with a 32-element Ge fluorescence detector and a beam size of about 2·2,5 mm.

Copper K-edge (8979 eV) and Zn K-edge (9656 eV) spectra were collected with 30% detuning whereas Fe-K edge (7112 eV) spectra were collected with 50% detuning. To reduce fluorescence and scattering from other elements a filter (Ni 3λ filter for Cu, Cu 3λ filter for Zn and Mn 3λ filter for Fe), Al foil and Soller slits were placed between the sample and the Ge detector.

Zinc K-edge spectra on MIBA samples G-A, G-A_pH 8.5, G-A_pH 6.5 and G-B were collected at beamline 4-3, equipped with a liquid N_2-cooled Si(1 1 1) monochromator. These spectra were collected at room temperature by a Lytle fluorescence detector with a Cu 3λ filter placed in front of the detector. For all measurements, metal foil were used as energy references and collected simultaneously.

XAS data collected at beam line 4-1 were deadtime corrected using SixPACK (Webb, 2005) before further data treatment. All spectra were then treated in the program package Demeter including Athena and Artemis vers. 0.9.26 (Ravel and Newville, 2005), with FEFF vers. 6 (Rehr and Albers, 2000). Energy calibration, averaging and background removal were performed according to procedures described by Kelly et al. (2008) including improvement of the background correction by a model of the first shell (set up in Artemis) for Cu and Zn. The background was removed using the AUTOBAK algorithm in Athena, with a *k*-weight of 2 or 3 and the Rbkg parameter set to 1. The shell-fitting procedure was

Table 1
Copper and zinc species suggested to be present in (MI)BA.

Suggested form/Mineral	Method for identification	Reference(s)
Cu(II) oxide (Tenorite, CuO)	XRD, EPMA	(Bayuseno, 2006)
	XAS	(Lassesson and Steenari, 2013)
	XAS	(Olsson et al., 2009)
	TEM, SEM-EDS + XRD	(Meima and Comans, 1999)
Cu(I) oxide (Cuprite, Cu_2O)	XAS	(Lassesson and Steenari, 2013)
	XRD, (probable form)	(Meima and Comans, 1999)
$Cu_2(OH)_3Cl$	XRD	(Piantone et al., 2004)[a]
$Pb_4Cu_4O_4Cl_8\cdot5H_2O$	XRD	(Piantone et al., 2004)[a]
$Cu_{19}Cl_4SO_4(OH)_{32}\cdot20H_2O$	XRD	(Piantone et al., 2004)[a]
Cu_2S	XRD	(Bayuseno, 2006)
CuS	XRD	(Bayuseno, 2006)
$Cu_{11}(OH)_{14}(CrO_4)_4$	XRD	(Piantone et al., 2004)[a]
$CuCr_2O_4$	XAS	(Lassesson and Steenari, 2013)
Cu metal (or alloy)	XAS	(Lassesson and Steenari, 2013)
	SEM-EDS	(Meima and Comans, 1999)
	SEM-EDX	(Wei et al., 2011)
Malakite ($Cu_2(OH)_2CO_3$)	Geochemical model	(Dijkstra et al., 2006)
Cu adsorption to Fe/Al-hydroxides	Geochemical model Geochemical model	(Dijkstra et al., 2006)
		(Meima and Comans, 1999)
Cu substitution in different minerals	Crystal-chemical data and XRD	(Piantone et al., 2004)[a]
Zn(II) oxide (zincite, ZnO)	SEM-EDS + XRD	(Meima and Comans, 1999)
	XRD, SEM	(Piantone et al., 2004)[a]
	XAS	(Steenari and Norén, 2008)
$Zn_2P_2O_7$	XRD	(Tang et al., 2015)
$Zn_2(PO_4)(OH)$	XRD	(Piantone et al., 2004)[a]
$Mn_2Zn(PO_4)_2$	XRPD	(Crannell et al., 2000)[b]
$Zn_3(PO_4)_2$	XRPD	(Crannell et al., 2000)[b]
$Zn_3(PO_4)_2\cdot4H_2O$	XRPD	(Crannell et al., 2000)[b]
$ZnFe_2(SO_4)_4$	XRD	(Piantone et al., 2004)[a]
$Cu_2Zn_4Al_2(OH)_{16}CO_3\cdot4H_2O$	XRD	(Piantone et al., 2004)[a]
Willemite (Zn_2SiO_4)	Geochemical model	(Dijkstra et al., 2006)
	XAS	(Steenari and Norén, 2008)
Zn(II) hydroxide ($Zn(OH)_2$)	XAS	(Steenari and Norén, 2008)
Zn metal	SEM-EDS	(Meima and Comans, 1999)
Zn adsorption to or surface precipitates on Fe/Al-hydroxides	Geochemical model	(Dijkstra et al., 2006)
		(Meima and Comans, 1999)
Zn substitution in different minerals	Crystal-chemical data and XRD	(Piantone et al., 2004)[a]
Zn in solid solution with carbonates	Mapping by microprobe	(Piantone et al., 2004)[a]

[a] Only secondary phases are studied.
[b] Phosphate was added to form precipitates with heavy metals in this study. Only Zn-species that were identified before phosphate addition are included in the list.

Table 2
Bottom ash samples and elements studied with XAS.

Sample	Incineration technique	Carbonation	XAS measurement
G-A	Grate fired boiler	Laboratory, 3 weeks[b]	Zn, Cu, Fe
G-A_pH 8.5[a]	Grate fired boiler	Laboratory, 3 weeks[b]	Zn
G-A_pH 6.5[a]	Grate fired boiler	Laboratory, 3 weeks[b]	Zn
G-B	Grate fired boiler	Naturally, outdoors[c]	Zn, Cu, Fe
G-C	Grate fired boiler	Naturally, outdoors[c]	Zn, Cu
FB-D	Bubbling fluidized bed	Naturally, outdoors[c]	Zn, Cu
G-E	Grate fired boiler	Naturally, outdoors[c]	Zn, Cu
G-F	Grate fired boiler	Naturally, outdoors[c]	Zn, Cu

[a] Solid residues of sub-samples of G-A leached at pH 8.5 and 6.5 according to EN 14997:2015.
[b] A 1–2 cm thick layer was kept in contact with air, watered and stirred 4 times during 3 weeks.
[c] The ash was placed in large heaps and naturally weathered i.e. not sheltered against wind and water for at least 4 months. After about 1–3 months metal pieces larger than ~2 mm were mechanically sorted out using magnets and/or eddy current magnets in stationary or mobile sorting equipment from the grate fired ashes. The exact size sorting capacity depends on the unique equipment.

performed on the Fourier transform real part of 1, 2, 3-*k*-weighted EXAFS spectra using a Hanning window (dk value = 1). The number of variables was much less than number of independent points. Copper spectra were modelled based on the structure of Cu metal (Wyckoff, 1963). Cu(II) oxide (tenorite) (Tunell et al., 1935), and Cu_2O (Hafner and Nagel, 1983), whereas Zn spectra were modelled based on Zn(II) oxide (Kihara and Donnay, 1985), Zn_2SiO_4 (willemite) (Klaska et al., 1978), and $ZnAl_2O_4$ (gahnite) (Ardit et al., 2012). Goodness-of-fit was evaluated by the R factor in Artemis. During the fitting procedure, the amplitude reduction factor (S_0^2) was set based on fitting of this parameter for the first coordination shell for Cu whereas for Zn it was set to the fit of standard ZnO. Some of the standards in Table S1 (Zn-standards from Medas et al. (2014), Cu(II) oxide from Lassesson and Steenari (2013), and Cu metal were evaluated using shell-fitting by the same method as bottom ash spectra to facilitate comparison of fitting parameters.

Atomic distances (R), number of back-scatters (coordination number, CN) and the Debye-Waller-factors (σ^2) were all fitted for the first coordination shell. For Zn spectra, σ^2 was set to 0.008 Å² for higher shells, based on results for the Zn(II) oxide standard. For Cu spectra, the σ^2 of higher shells were set to the value achieved for the standards Cu(II) oxide and Cu metal (with some exceptions).

Iron spectra were evaluated by comparison to a collection of standard spectra available from MAX-lab in Lund, Sweden, collected at former beamline I811.

2.4. pH dependent leaching tests

pH-dependent leaching tests were performed on two of the MIBA: G-A and G-B. These tests were performed at four different pH values for 48 h according to SS-EN 14997:2015 with some modifications, primarily particle size 0.25 mm instead of 1 mm and L/S ratio ~100 instead of 10. pH was continually measured with a gel electrode (Hamilton Polylite) and adjusted with HNO_3 to pH 5.5, 6.5, 7.5, and 8.5. In addition, as the pH electrode may leach some K, Cl and DOC (dissolved organic carbon) one subsample of each ash was leached without continuous pH measurement and adjustment but with initial HNO_3 addition aiming at pH 7.5.

Leachates were analysed for metals and cations according to SS-EN ISO 17294-2 or SS-EN ISO 11885 after filtering through 0.45 μm filters and acidification with HNO_3. DOC was analysed on filtered leachates according to SS-EN ISO 1484.

2.5. Extraction of Fe, Al, Cu, and Zn

The amounts of poorly crystalline Fe and Al hydroxides in G-A, G-B, G-C and FB-D were estimated from extraction with ammonium oxalate, SS-EN ISO 12782-1. The results for G-A and G-B were used to calculate the concentration of poorly crystalline Al and Fe hydroxides that can adsorb Cu and Zn in the geochemical model simulations (Section 2.6).

Extractions at pH 1.2 and L/S 96 during 32 h were also performed. Samples with particle size <0.063 mm were mixed with deionized water and continuously stirred with pH controlled to 1.2 ± 0.1 pH units by HCl (6 M) addition (T9 titrator from Mettler Toledo and gel electrode Hamilton Polylite). The concentrations of Cu and Zn in the leachate give input to estimation of the "geochemically active" concentrations, i.e. the concentrations that take part in chemical equilibrium reactions (Groenenberg and Lofts, 2014) and were used as input data in the geochemical modelling (Section 2.6).

2.6. Geochemical equilibrium modelling

The free-ware Visual MINTEQ, version 3.1 (Gustafsson, 2013) was used for geochemical equilibrium simulations. Modelling results were compared to results from the pH-dependent leaching test. Three types of calculations were performed:

(1) Investigation of Cu and Zn sorption to hydroxide minerals and organic matter. A multi surface (or assemblage) model was set up (Groenenberg and Lofts, 2014). It included speciation in the solute, sorption/desorption to Fe and Al hydroxide (HFO) surfaces and complexation with solid organic matter (SOM). The parameterized "sub models" for reactions with HFO and SOM in Visual MINTEQ were used without changes, i.e. the model was not calibrated.

(2) Identification of minerals with documented solubility products (K_s). Calculated Cu^{2+} (aq) and Zn^{2+} (aq) concentrations from dissolution of different minerals were compared to measured concentrations in pH-dependent leaching tests. Mineral solubility was calculated with concentrations of DOC, macroions (Ca, K, Na, Mg, Mn, Fe, Cl, SO_4, NO_3, PO_4, CO_3, Si) and pH in the leachates.

(3) Indication of solubility-controlling minerals by calculation of ion activity products (IAP). For a few minerals, e.g. hardystonite and hemimorfite, identified as candidate minerals in MIBA but for which K_s were lacking, ion activity products (IAP) in the pH-dependent leachates were calculated

instead. A relatively constant IAP within 2 log units within the pH interval indicates that the mineral is present and may govern the concentrations in solution.

More details are given in the Supplementary material, Table S2–S5.

3. Results

3.1. Characterization of bottom ash samples

The concentrations of Cu, Zn, Fe, Al, and Si in the original ash samples are presented in Table 3. The Cu content ranged from about 0.2 to 0.8% and Zn from 0.4 to 0.6%. The grate boiler ashes contained 8–11% Fe, 5–6% Al and 17–20% Si. Due to the addition of sand in the combustion process, the fluidized bed BA contained more Si, here 26%.

All ashes were alkaline with pH between 9.4 and 11 (Table 3). The content of organic carbon was below or equal to 0.5% in all ashes except G-C, which contained 1.2% organic carbon. Inorganic carbon was between 0.1 and 0.9% (Table 3). The fractions of Cu and Zn that were extracted at pH 1.2 varied between the tested ashes (G-A, G-B, G-C and FB-D, Table S6); Cu: 37–61% and Zn: 25–80% of the total content.

The main minerals in the MIBA identified by XRD were essentially the same although the proportions differed slightly (Table 4; Fig. S1). The most abundant minerals were quartz and feldspar but there was also a significant amount of poorly crystalline or amorphous material. Iron minerals magnetite and hematite were present, whereas no Cu or Zn containing minerals were identified, which was expected due to the low total amounts of those elements. The silicate mineral $Ca_2MgSi_2O_7$ (akermanite) was present in all ashes.

Adsorption to iron oxides/hydroxides (especially poorly crystalline) has been suggested to be one important retention mechanism for Cu and Zn in bottom ash (Dijkstra et al., 2006; Meima and Comans, 1999). Iron EXAFS spectra were therefore collected for two ashes, G-A and G-B (Fig. 1). The two ash spectra have very similar form, so they should contain similar species. When comparing transmission and fluorescence spectra (not shown) the fluorescence signal was slightly attenuated, indicating self-absorption. However, the phase of the EXAFS spectra is not affected, and they resembled the minerals hematite and magnetite suggested by XRD and ferrihydrite, which may be part of the amorphous minerals identified with XRD (>10%). Oxalate extractable iron can be used to estimate the amount of poorly crystalline iron (hydr)oxides (i. e ferrihydrite; (Parfitt and Childs, 1988)). The oxalate extractable Fe fractions in ashes G-A, G-B, G-C and FB-D were about 20% (Table S6) indicating that a considerable part of Fe may be poorly crystalline phases. In summary, the bottom ashes probably contain a mixture of different iron minerals, with hematite, magnetite, and amorphous iron oxide/hydroxide as important constituents.

3.2. EXAFS analysis of copper and zinc

Copper EXAFS spectra for the MIBA were similar, indicating similar speciation in the ashes (Fig. 2a). However, the spectrum for one of the grate boiler ashes, G-A, and the fluidized bed ash, FB-D, had a slightly larger amplitude compared to the other ashes. The MIBA spectra did not obviously match any of the Cu standard spectra and the ashes probably contained a mixture of phases.

An analysis of the first shell designated both Cu–O and Cu–Cu distances, while for example Cu–S and Cu–Cl distances were lacking. The Cu–O distance of 1.92–1.93 Å in all ashes was near the typical Cu(II)-O distance of 1.95 Å (Table S7). This distance is the first

Table 3
Total content of Cu, Zn, Fe, Al and Si as well as pH, TOC and TIC in the BA samples. Average concentrations from double (*) or triple (+) replicates. Standard deviation within brackets.

BA	Cu g/kg dw	Zn g/kg dw	Fe g/kg dw	Al g/kg dw	Si g/kg dw	pH[a]	TOC (%)	TIC (%)
G-A	6.5 (1.1)[+]	5.9 (0.1)[+]	103 (4.7)[+]	57 (1.4)[+]	173 (4.7)[+]	9.4 (0.4)*	0.4 (0.1)[+]	0.9 (0.0)[+]
G-B	7.8 (0.6)[+]	4.6 (0.1)[+]	110 (0)[+]	47 (1.7)[+]	190 (8.2)[+]	10.0 (0.1)*	0.4 (0.0)[+]	0.5 (0.0)[+]
G-C	3.6 (0.3)*	4.9 (0.3)*	76 (2)*	56 (0.5)*	190 (0)*	9.4	1.2 (0.0)*	0.9 (0.01)*
FB-D	4.7 (0.2)*	3.7 (0.1)*	48 (0.5)*	40 (0.5)*	265 (5)*	11	<0.2 (0.0)*	0.1 (0.0)*
G-E	2.7 (0.2)*	4.4 (0.3)*	105 (5)*	51 (0.5)*	205 (5)*	10.8	0.3	0.4
G-F	2.4 (0.3)*	4.0 (0.5)*	97 (3)*	56 (5)*	165 (15)*	10.4	0.5	0.4

[a] G-A, G-B, G-E and G-F pH according to EN 15933, G-C and FB-D in leachate at L/S 10 (EN 12457-2).

Table 4
Minerals in bottom ash. Results from XRD measurements.

Mineral	G-A	G-B	G-C	FB-D	G-E	G-F
Quarts, SiO_2	Major	Major	Major	Major[b]	Medium	Major
Feldspar[a]	Medium	Medium	Medium	Medium	Medium	Medium
Calcite, $CaCO_3$	Minor	Minor	Minor	Minor	Minor	–
Magnetite, Fe_3O_4	Minor	Minor	Minor	Minor	Minor	Minor
Hematite, Fe_2O_3	Minor	Trace	Minor	Minor	Minor	Minor
Akermanite, $Ca_2Mg(Si_2O_7)$	Minor	Minor	Minor	Trace	Minor	Minor
Muscovite, $KAl_2[AlSi_3O_{10}](OH,F)_2$	–	Trace	Trace	Trace	Medium	–
Amorphous minerals	>10%	>10%	>10%	<10%	>10%	>10%

[a] Albite, microcline, anorthite and anorthoclase.
[b] Predominant.
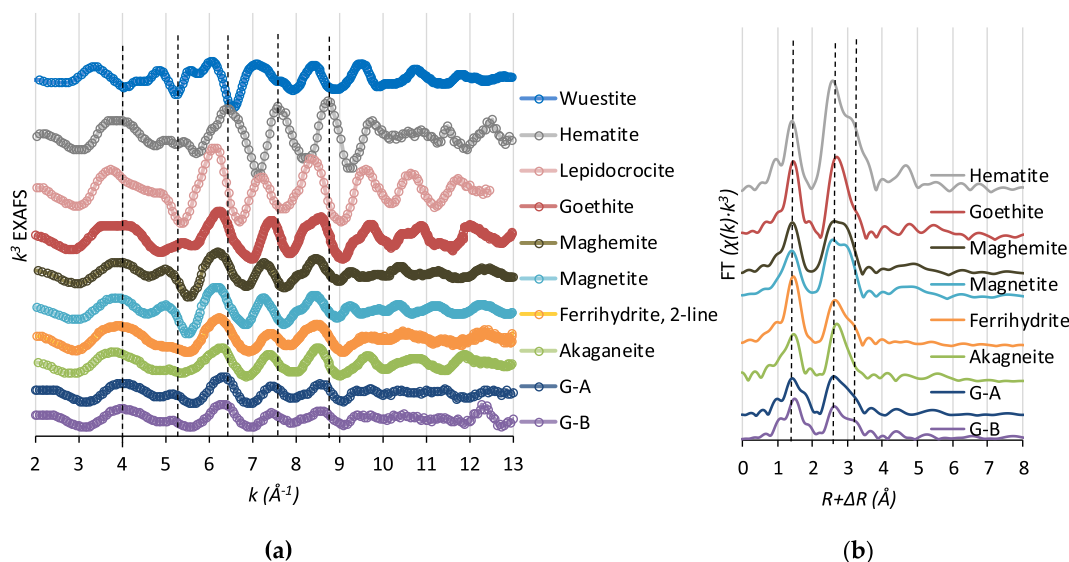
Fig. 1. Results from EXAFS measurements: (**a**) k^3-weighted Fe EXAFS spectra of standards and MIBA; (**b**) Fourier transforms of k^3-weighted Fe EXAFS spectra. The first dashed vertical line marks a Fe-O distance, the second and third Fe···Fe distances (FT not phase corrected).

peak in the Fourier Transform (FT, Fig. 2b). The Cu-O distance together with higher shell Cu···Cu distances of ~3.4–3.5 Å, ~3.7 Å, and in some samples ~4.7 Å, identified Cu(II) oxide (tenorite) in the ashes. However, to explain the magnitude of the second peak in the FT a Cu–Cu distance of 2.52–2.57 Å had to be added. This is a distinctive characteristic of Cu metal (Table S7) and displays that a significant part was metallic, Cu(0). Several samples also contained a Cu···Cu distance of ~4.45 Å present in Cu metal. Consequently, the EXAFS analysis indicated that the main Cu species in all examined MIBA were Cu(II) oxide and Cu metal. Bottom ashes G-A and FB-D contain more Cu metal, evidenced by a higher Cu–Cu coordination number (Table S7) and a higher peak in the FT (Fig. 2b). Other minerals and/or Cu adsorbed to metal hydroxides (e.g. ferrihydrite) or organic matter may also be present in small amounts in all bottom ashes.

As Cu metal contains a characteristic Cu-Cu distance, the content of Cu metal could be estimated from the number of backscatters (CN, Table S7). Based on the coordination number of the 2.55 Å Cu–Cu distance in the Cu metal standard compared to the CN of this distance in the bottom ashes 9–43% of Cu was metallic (including 30% uncertainty of CN). Bottom ashes G-A and FB-D contained more Cu metal (21–43%) than other ashes, consistent with EXAFS spectra and FT closer to the Cu metal standard in Fig. 2.

Zinc spectra for G-A, G-B, G-C and G-F (Fig. 3) were in general very similar in shape, which implies a similar Zn speciation in these MIBA although spectra for one grate boiler ash, G-E, and the fluidized bed ash, G-FB, were slightly different. The ash spectra do not obviously resemble any of the Zn standard spectra indicating a mixture of different phases or a phase not present in the standards, such as an amorphous mineral form. The spectrum from the
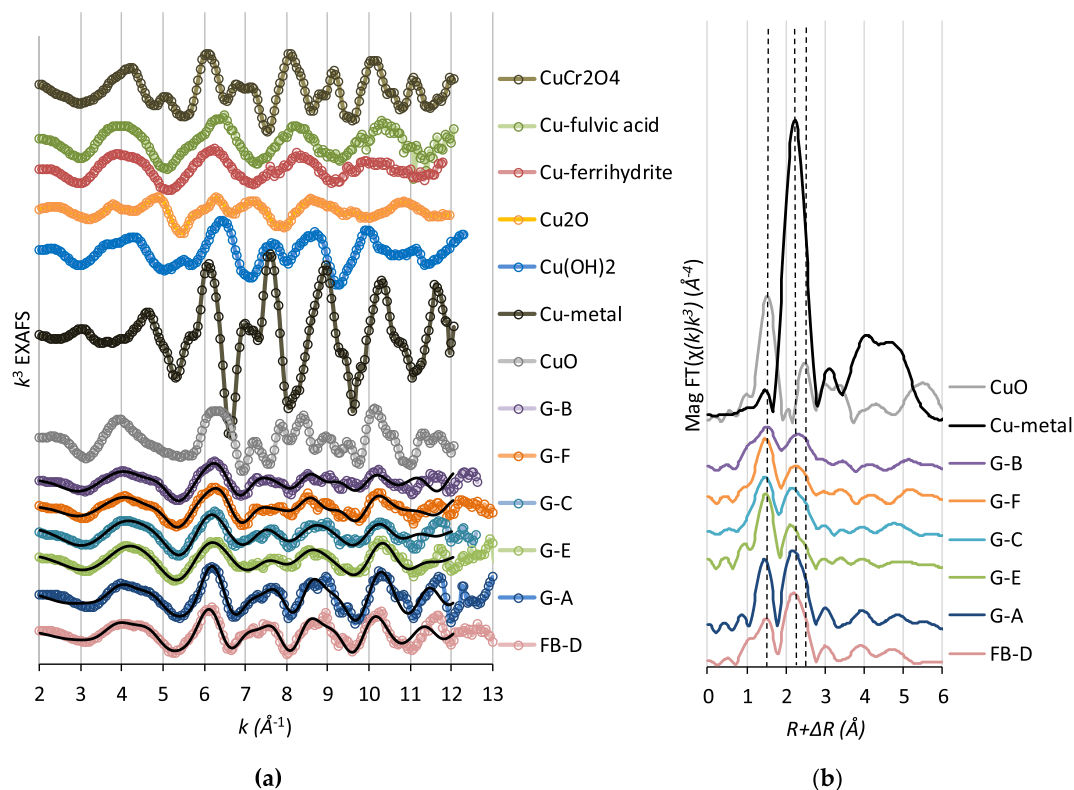
Fig. 2. Results from EXAFS measurements: (**a**) k^3-weighted Cu-EXAFS spectra of standards and MIBA, black solid lines are fits (only ashes); (**b**) Fourier transforms of k^3-weighted Cu-EXAFS spectra. The first dashed vertical line marks a Cu-O distance in CuO, the second and third Cu···Cu distances in Cu-metal and CuO, respectively (FT not phase corrected).

ash sample that was leached at pH 8.5 (G-A_8.5) was very similar to the spectrum for the original G-A ash, while the sample leached at pH 6.5 (G-A_6.5) has lost some features indicating that one or more Zn-species dissolved during leaching.

A Zn–O distance of 1.96–1.99 Å was identified in all ash samples (Table S8), showing Zn(II) bound to oxygen in the first shell, mainly in a tetrahedral configuration (Waychunas et al., 2002). There were no Zn-S or Zn-Cl distances present in the first shell excluding such phases. Significant amounts of $ZnCO_3$ and hydrozincite ($Zn_5(CO_3)_2(OH)_6$) could also be excluded based on the fact that Zn has a partly octahedral Zn-O configuration in these minerals, giving a longer Zn-O distance (2.03–2.11 Å; (Lee et al., 2005; Medas et al., 2014)). In the higher shells, a Zn···Zn distance of ~3.2 Å was identified in all and a Zn···Zn distance of about 4.5 Å in several grate boiler ashes. Both these distances are consistent with Zn(II) oxide and willemite (Zn_2SiO_4) (Table S8), and the corresponding peaks are marked in the FT (Fig. 3b). None of the MIBA spectra obviously resembled Zn(II) oxide or willemite, but similar spectral features with lower amplitude could be found (Fig. 3a) which may indicate that forms in the MIBA are more amorphous than the standards. Samples G-C and G-F were similar to the Zn(II) oxide and most likely contained this species. Since the amplitude for the FT peak representing the 3.2 Å distance is smaller than for Zn(II) oxide but larger than for willemite (Fig. 3b) the coordination number is in between the two standards, suggesting a mixture. Also, a ~3.4 Å Zn···Zn distance was identified in some samples and may be attributed to hemimorphite ($Zn_4Si_2O_7(OH)_2$; Table S8) or ε-Zn$(OH)_2$ (Jacobs et al., 2005).

The fluidized bed ash, FB-D, did not have the clear Zn···Zn distance at 3.2 Å present in the grate boiler ashes. Instead a Zn···Zn distance at 3.5 Å was identified, which, together with the Zn-O distance may be franklinite ($ZnFe_2O_4$) or gahnite ($ZnAl_2O_4$) (Steenari and Norén, 2008). A Zn···Si distance of ~3.0–3.1 Å improved the

fit of FB-D indicating some Zn-silicate mineral. This Zn···Si distance is present in minerals like willemite (Steenari and Norén, 2008), hardystonite (Louisnathan, 1969), and hemimorphite (Ziegler et al., 2001). Some of the other measured MIBA Zn EXAFS spectra also contain contributions from "light" backscatters (e.g. Mg, Al, Si) in higher shells, but as these give weaker signals in the EXAFS measurement compared to "heavy" backscatters (e.g. Cu, Zn, Fe) they are difficult to identify clearly. Hardystonite, for example, has no heavy backscatters closer than 5 Å to the central atom, which would be difficult to distinguish in an ash spectrum. Furthermore, no EXAFS spectrum of this mineral is present in the literature to compare with.

Consistent with the lower EXAFS amplitude of G-A_6.5 compared to G-A, the number of backscatters at 3.2 Å decreased after leaching, from 3.1 in the original G-A to 2.2 in G-A_8.5 and only 0.5 in G-A_6.5. This can also be seen in the FT (Fig. 3b), where the second peak in the FT has almost disappeared in G-A_6.5 showing that some mineral(s) has dissolved. When one mineral dissolves, other phases may be easier to distinguish. After leaching at 6.5 (G-A_6.5) the 3.0 Å Zn···Si and the 3.4 Å Zn···Zn distances, consistent with hemimorphite, could be added in the shell-fitting, although with low CN. It is also possible that some of the Zn was adsorbed to iron oxides, e.g. ferrihydrite, since that phase also has a low number of backscatters.

3.3. pH dependent leaching and geochemical modelling

Concentrations of Cu^{2+} (aq) and Zn^{2+} (aq) ions, calculated from dissolved Cu and Zn in leachates of G-A and G-B at pH 5.5, 6.5, 7.5, and 8.5, are presented in Fig. 4 together with geochemical simulations. The solubility of both Cu and Zn decreased with higher pH, which was expected as their adsorption to Fe and Al hydroxides (HFO) as well as complexation to organic matter (SOM,
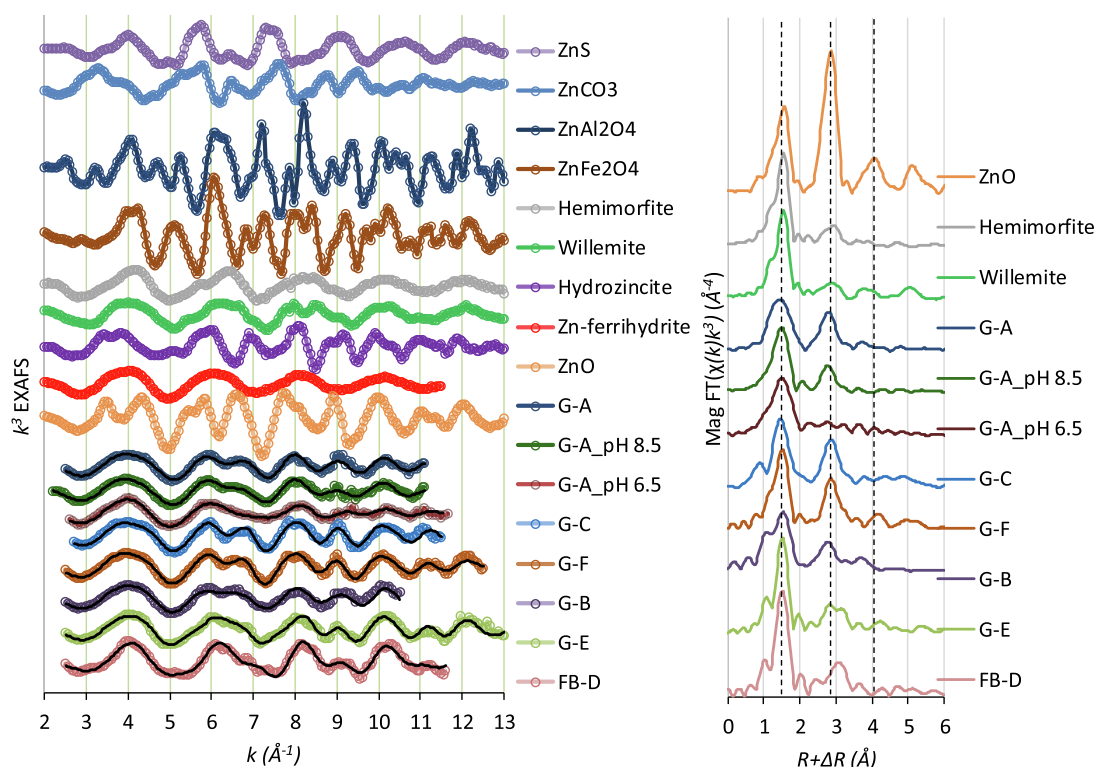
Fig. 3. Results from EXAFS measurements: (**a**) k³-weighted Zn-EXAFS spectra of standards and MIBA, black solid lines are fits (only ashes); (**b**) Fourier transforms of k³-weighted Zn-EXAFS spectra. The first dashed vertical line marks a Zn-O distance at ~2.0 Å. The second and third lines are Zn···Zu distances at ~3.2 and ~4.6 Å (the FT is not phase corrected).

DOM) increases with pH in this interval and oxides and hydroxides may precipitate at high pH.

The black lines in Fig. 4 are results from simulation of sorption/complexation to HFO and SOM. This simulation greatly overestimated Cu^{2+} (aq) and Zn^{2+} (aq) concentrations at pH above ~6.5, which indicates that they were governed by other processes at high pH, possibly equilibrium with minerals. Equilibrium Cu^{2+} and Zn^{2+} concentrations of candidate minerals (based on the EXAFS analysis) with available solubility constants were compared to leachate concentrations. As the ashes were carbonated and malachite ($Cu_2(OH)_2CO_3$) has been suggested based on geochemical modelling (Dijkstra et al. 2006), solubility of malachite, zinc-carbonate ($ZnCO_3$), and hydrozincite ($Zn_5(CO_3)_2(OH)_6$) were also calculated. Minerals are represented by dashed lines in Fig. 4. Concentrations close to experimental results indicate that the mineral governs the concentration in solution. Minerals giving consistently lower concentrations than leachate concentrations are stable and may be present but does not regulate the concentration in the leachate. Minerals giving higher concentrations are not thermodynamically stable and dissolves (if not occluded in other minerals or dissolution is very slow). For two candidate minerals from the EXAFS analysis, hardystonite ($Ca_2ZnSi_2O_7$) and hemimorfite ($Zn_4Si_2O_7(OH)_2·H_2O$), no solubility constants could be found and therefore IAP was calculated instead. The log IAP calculations did not indicate hardystonite since log IAP ranged between 18 at pH 5.5 and 30 at pH 8.5 for both ashes and the difference was always >2 log units between 2 pH units. For hemimorfite log IAP ranged from 21–22 (pH 5.5) to 31 but differed only 1 log unit between 7.5 and 8.5, indicating that hemimorphite may be present. Solubilities of Cu_2O and $CuCr_2O_4$ were not investigated as they contain reduced forms of Cu or Cr (Cu(I) and Cr(III)) and the conditions during leaching (and carbonation) were oxidizing. Solubility of Cu metal is low at the studied conditions.

The geochemical simulations indicated that Cu and Zn concentrations in leachates may be controlled by adsorption/complexation to HFO and SOM at low pH (to about pH 6) and by minerals in equilibrium with the water phase at higher pH. For Cu a more crystalline form of tenorite was the best candidate, supporting the EXAFS measurements. However, concentrations in leachate from G-A were still overestimated. Willemite solubility followed Zn in leachate closely in large part of the interval, strongly suggesting a form of this phase to be present in the ashes. These results are in line with earlier modelling studies (Dijkstra et al., 2006; Meima and Comans, 1999) that also suggested sorption, tenorite, and willemite to constrain the Cu and Zn concentrations in BA leachate.

4. Discussion

4.1. Copper in bottom ash

The EXAFS measurements together with geochemical modelling strongly indicated presence of Cu(II) oxide as has also been suggested in more than half of the Cu-studies listed in Table 1. In addition, the EXAFS analysis distinguished Cu metal in all ashes and this fraction was larger in FB-D and G-A (with 21–43% of Cu as Cu metal) than in the other ashes. In earlier XAS studies Cu metal was identified in an uncarbonized FB ash (Lassesson and Steenari, 2013) but not in a MIBA grate boiler ash (Olsson et al., 2009). The XRD analysis did not identify any Cu containing minerals, which was not expected due to the low Cu content in the samples.

4.2. Zinc in bottom ash

EXAFS indicated a similar Zn speciation in the ashes. Zn(II) oxide and willemite, were identified as possible major Zn species
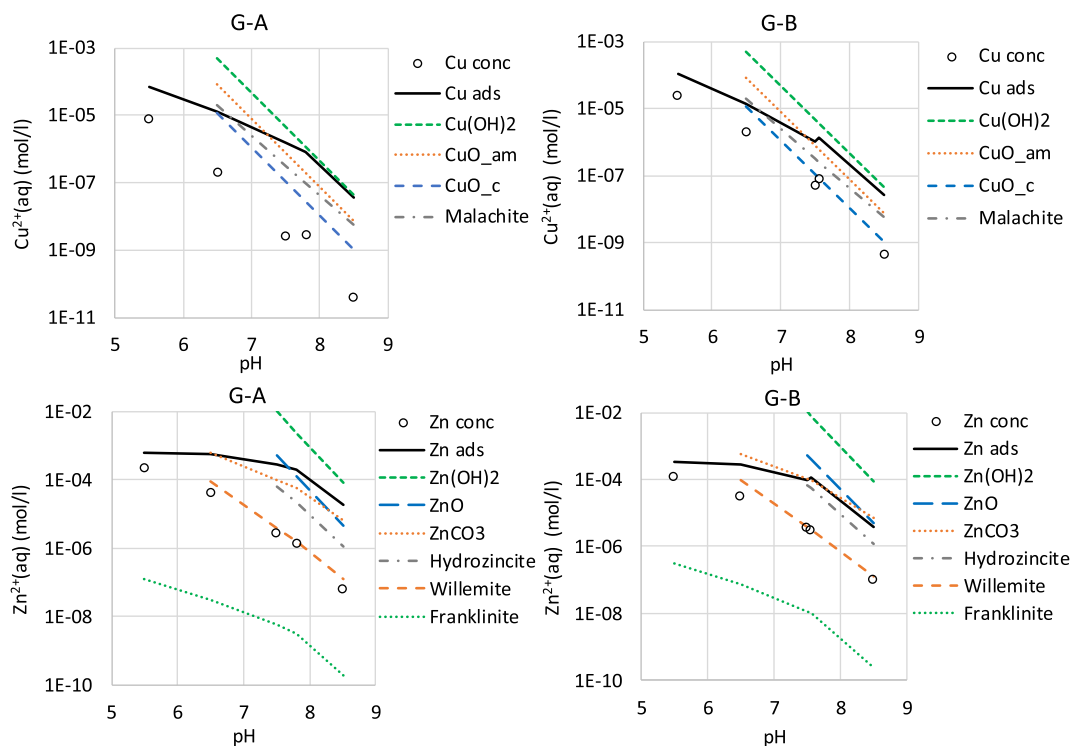
Fig. 4. pH-dependent solubility of $Cu^{2+}(aq)$ and $Zn^{2+}(aq)$. pH-dependent leaching (circles) and simulation of concentrations if governed by adsorption (black solid line). Simulated solubility of Cu and Zn minerals: $Cu(OH)_2$ (Cu hydroxide), CuO_am (amorphous Cu(II) oxide), CuO_c (crystalline Cu(II) oxide), malachite ($Cu_2(CO_3)(OH)_2$), $Zn(OH)_2$ (zinc hydroxide), ZnO (Zinc(II) oxide), $ZnCO_3$, hydrozincite ($Zn_5(CO_3)_2(OH)_6$), willemite (Zn_2SiO_4) and franklinite ($ZnFe_2O_4$) (dashed lines).

in the grate boiler ashes. Both these species have earlier been suggested for BA (Table 1). Modelling of willemite solubility matched data from the pH dependent leaching test particularly well and the mineral dissolved during leaching at pH 6.5 may therefore be willemite (Meima and Comans, 1999). It is also therefore highly likely that willemite was present in the ashes G-A and G-B. The fact that the MIBA spectra does not obviously resemble the willemite standard indicates that the form may be less crystalline. Regarding Zn (II) oxide, it was not stable within the pH range of the leaching tests but it could be at the original pH (>9.4 in all ashes). Presence of hemimorphite was also indicated, although more uncertain, by both EXAFS and IAP calculations. For the fluidized bed ash, FB-D, EXAFS data indicates Si-mineral(s) but also franklinite ($ZnFe_2O_4$) or gahnite ($ZnAl_2O_4$).

XRD identified akermanite in all ashes. This is interesting because akermanite is part of the melilite mineral group which includes $Ca_2ZnSi_2O_7$ (hardystonite) where Mg is substituted for Zn. Hardystonite has been identified in MSWI fly ash (Liu et al., 2009). It is therefore a possibility that hardystonite is present in the ashes (but in concentrations too low to be detected by XRD). However, its presence in the current study was neither confirmed nor discarded by EXAFS (standard is lacking) or geochemical calculations (solubility product is lacking).

4.3. EXAFS for analysis of MIBA

The EXAFS measurements showed that speciation of Cu and Zn was similar in different ashes. If spectra have the same form they also contain the same main species. This is important information for the possibility to generalize hazard and risk assessment of metals in ashes. Similar spectra from different ash samples also indicate that it is possible to obtain representative samples despite the inhomogeneity of MIBA. Copper species were easier to identify in MIBA than Zn species. Experience from the performed EXAFS

measurements show that Zn was more associated with light backscatters compared to Cu, which complicates interpretation of Zn EXAFS spectra. This is emphasized by the variety of earlier suggested Zn species in Table 1.

A success factor when it comes to understand speciation is to use several complementary methods in the analysis. In this study we combined EXAFS, XRD, pH dependent leaching, extractions, and geochemical equilibrium modelling. All analyses provided important information and they were also consistent with each other, which gives a stronger support to the conclusions. Complementary analysis for an even better understanding could be obtained for example by μ-XRF to get a picture of the spatial distribution and co-occurrence of elements combined with μ-EXAFS on selected spots to be able to easier identify specific species. More measurements could also be made on samples leached at different pH values, since when one species is dissolved, it is easier to distinguish other species. More studies on solubility products of Zn minerals are also of interest.

5. Conclusions

In summary, we could conclude that Cu(II) oxide and Cu metal were the main Cu species in all investigated ashes. The content of Cu metal could be quantified to range between 10 and 40% of total Cu in the ashes. A minor part of the Cu was present in other forms; in minerals or adsorbed.

For Zn, our data confirms willemite and Zn(II) oxide as main Zn species in the investigated grate boiler ashes, possibly as amorphous forms. Franklinite/gahnite and Si-minerals were probably main minerals in the fluidized bed ash. There were indications of hemimorphite and possibly hardystonite in both types of ashes.

Finally, we want to emphasize the importance of using complementary techniques and multiple lines of evidence to understand speciation.

6. Implications

The findings have, in addition to increasing the general knowledge about speciation of Cu and Zn in MIBA, implications for classification of MIBA. Classification of e.g. HP 14 should be based on the presence of specific compounds in the material (e.g. ZnO, franklinite or other mineral) but as the speciation of most elements in MIBA is poorly known the assessment is often based on "worst case" assumptions (i.e. Zn present as ZnO). With increased knowledge about the actual speciation, uncertainty in the classification decreases.

The identified species and leaching tests show that leaching will be governed by dissolution of minerals, probably tenorite and willemite. These suggested main species are stable above neutral pH, which limits concentrations in leachate as long as pH does not drop drastically. Under natural conditions pH in MIBA will be alkaline for a long time. This means that leaching of Cu and Zn is predictive and can be assessed against set criteria and timeframes for risk assessment.

As the speciation in grate boiler ashes was similar, we expect the results to be representative for metal separated and "aged" bottom ashes from large scale grate boiler incineration of municipal and industrial solid waste.

Unfortunately, it is not possible to give more specific guidance on implications for classification and re-use of MIBA as the (implementation of) legislation and regulations differ between countries. For example, hazard classification of MIBA within the European union should be based on the Waste Framework Directive (European Parliament and Council, 2008) but clear guidance is lacking, and practice differ between countries.

Declaration of Competing Interest

The authors declare that they have no known competing financial interests or personal relationships that could have appeared to influence the work reported in this paper.

Acknowledgements

Appendix A. Supplementary material

Supplementary data to this article can be found online at https://doi.org/10.1016/j.wasman.2020.10.023.

References

Ardit, M., Cruciani, G., Dondi, M., 2012. Structural relaxation in tetrahedrally coordinated Co2+ along the gahnite-Co-aluminate spinel solid solution. Am. Mineral. 97, 1394–1401.

Arickx, S., Van Gerven, T., Vandecasteele, C., 2006. Accelerated carbonation for treatment of MSWI bottom ash. J. Hazard. Mater. 137, 235–243. https://doi.org/10.1016/j.jhazmat.2006.01.059.

Avfall Sverige, 2005. Svensk Avfallshantering 2018 (Swedish waste disposal 2018). Malmö.

Bayuseno, A.P., 2006. Mineral phases in raw and processed municipal waste incineration residues-towards a chemical stabilisation and fixation of heavy metals. Ruhr-Universität Bochum.

Blasenbauer, D., Huber, F., Lederer, J., Quina, M.J., Blanc-biscarat, D., Bogush, A., Bontempi, E., Blondeau, J., Maria, J., Dahlbo, H., Fagerqvist, J., Giro-paloma, J., Hjelmar, O., Hyks, J., Keaney, J., Lupsea-toader, M., Simon, F., Svecova, L., Joyce, C., Caollai, O., Orupõld, K., Paja, T., Šyc, M., Ulvang, R., Vaajasaari, K., Caneghem, J. V., Zomeren, A.V., Vasarevic, S., Wégner, K., Fellner, J., 2020. Legal situation and current practice of waste incineration bottom ash utilisation in Europe. Waste Manage. 102, 868–883. https://doi.org/10.1016/j.wasman.2019.11.031.

Crannell, B.S., Eighmy, T.T., Krzanowski, J.E., Eusden, J.D., Shaw, E.L., Francis, C.A., 2000. Heavy metal stabilization in municipal solid waste combustion bottom ash using soluble phosphate. Waste Manage. 20, 135–148. https://doi.org/10.1016/S0956-053X(99)00312-8.

Dijkstra, J.J., Van Der Sloot, H.A., Comans, R.N.J., 2006. The leaching of major and trace elements from MSWI bottom ash as a function of pH and time. Appl. .istry 21, 335–351. https://doi.org/10.1016/j.apgeochem.2005.11.003.

Dou, X., Ren, F., Nguyen, M.Q., Ahamed, A., Yin, K., Chan, W.P., Chang, V.W.C., 2017. Review of MSWI bottom ash utilization from perspectives of collective characterization, treatment and existing application. Renew. Sustain. Energy Rev. https://doi.org/10.1016/j.rser.2017.05.044.

European Parliament and Council, 2008. Directive 2008/98/EC of the European Parliament and of the Council of 19 November 2008 on waste and repealing certain directives (Waste framework. LexUriServ. do 9, 3–30. https://doi.org/2008/98/EC.; 32008L0098.

Freyssinet, P., Piantone, P., Azaroual, M., Itard, Y., Guyonnet, D., Baubron, J.C., 2002. Chemical changes and leachate mass balance of municipal solid waste bottom ash submitted to weathering. Waste Manage. 22, 159–172.

Groenenberg, J.E., Lofts, S., 2014. The use of assemblage models to describe trace element partitioning, speciation, and fate: A review. Environ. Toxicol. Chem. 33, 2181–2196. https://doi.org/10.1002/etc.2642.

Gustafsson, J.P., 2013. Visual MINTEQ 3.1. http://vminteq.lwr.kth.se/.

Hafner, S., Nagel, S., 1983. The electric field gradient at the position of copper in Cu2O and electronic charge density analysis by means of K-factorse. Phys. Chem. Miner. 9, 19–22.

Jacobs, H., Niemann, A., Kockelmann, W., 2005. Low temperature investigations of hydrogen bridge bonds in the hydroxides beta-Be(OH)2 and epsilon-Zn(OH)2 by Raman-spectroscopy as well as X-ray and neutron diffraction Locality: synthetic Sample: T = 298 K. Zeitschrift fur Anorg. und Allg. Chemie 631, 1247–1254.

Kelly, S., Hesterberg, D., Ravel, B., 2008. Analysis of soils and minerals using X-ray absorption spectroscopy. In: Ulery, A.L., Drees, R.L. (Eds.), Methods of Soil Analysis. Part 5. Mineralogical Methods. SSSA Book Series, SSSA, Madison, WI.

Kihara, K., Donnay, G., 1985. Anharmonic thermal vibrations in ZnO. Can. Mineral. 23, 647–654.

Klaska, K.-H., Eck, J.C., Pohl, D., 1978. New investigation of willemite. Acta Crystallogr. Sect. B 34, 3324–3325. https://doi.org/10.1107/S0567740878010778.

Kowalski, P.R., Kasina, M., Michalik, M., 2017. Metallic Elements Occurrences in the Municipal Waste Incineration Bottom Ash. Energy Procedia 125, 56–62. https://doi.org/10.1016/j.egypro.2017.08.060.

Lassesson, H., Steenari, B.M., 2013. Speciation of copper in ash from a fluidized-bed boiler fired with municipal solid waste. Energy Fuels 27, 3891–3897. https://doi.org/10.1021/ef400386j.

Lee, Y.J., Elzinga, E.J., Reeder, R.J., 2005. Sorption mechanisms of zinc on hydroxyapatite: Systematic uptake studies and EXAFS spectroscopy analysis. Environ. Sci. Technol. 39, 4042–4048. https://doi.org/10.1021/es048593r.

Liu, Y., Zheng, L., Li, X., Xie, S., 2009. SEM/EDS and XRD characterization of raw and washed MSWI fly ash sintered at different temperatures. J. Hazard. Mater. 162, 161–173. https://doi.org/10.1016/j.jhazmat.2008.05.029.

Louisnathan, S.J., 1969. Refinement of the crystal structure of hardystonite, Ca2ZnSi2O7. Zeitschrift fur Krist. 130, 427–437.

Medas, D., Lattanzi, P., Podda, F., Meneghini, C., Trapananti, A., Sprocati, A., Casu, M. A., Musu, E., De Giudici, G., 2014. The amorphous Zn biomineralization at Naracauli stream, Sardinia: Electron microscopy and X-ray absorption spectroscopy. Environ. Sci. Pollut. Res. 21, 6775–6782. https://doi.org/10.1007/s11356-013-1886-4.

Meima, J.A., Comans, R.N.J., 1999. The leaching of trace elements from municipal solid waste incinerator bottom ash at different stages of weathering. Appl. Geochem. 14, 159–171. https://doi.org/10.1016/S0883-2927(98)00047-X.

Olsson, S., Gustafsson, J.P., Berggren Kleja, D., Bendz, D., Persson, I., 2009. Metal leaching from MSWI bottom ash as affected by salt or dissolved organic matter. Waste Manage. 29, 506–512. https://doi.org/10.1016/j.wasman.2008.03.017.

Parfitt, R.L., Childs, C.W., 1988. Estimation of forms of Fe and Al-a review, and analysis of contrasting soils by dissolution and Mossbauer methods. Soil Res. 26, 121–144.

Piantone, P., Bodénan, F., Chatelet-Snidaro, L., 2004. Mineralogical study of secondary mineral phases from weathered MSWI bottom ash: Implications for the modelling and trapping of heavy metals. Appl. Geochem. 19, 1891–1904. https://doi.org/10.1016/j.apgeochem.2004.05.006.

Ravel, B., Newville, M., 2005. ATHENA, ARTEMIS, HEPHAESTUS: data analysis for X-ray absorption spectroscopy using IFEFFIT. J. Synchrotron Radiat. 12, 537–541. https://doi.org/10.1107/S0909049505012719.

Rehr, J.J., Albers, R.C., 2000. Theoretical approaches to X-ray absorption fine structure. Rev. Mod. Phys. 72.

Steenari, B.-M., Norén, K., 2008. Zinks förekomstformer i aska studerade med en röntgenabsorptionsspektrometrisk metod, Miljöriktig användning av askor.

Stiernström, S., Wik, O., Bendz, D., 2016. Evaluation of frameworks for ecotoxicological hazard classification of waste. Waste Manage. 58, 14–24. https://doi.org/10.1016/j.wasman.2016.08.030.

Tang, P., Florea, M.V.A., Spiesz, P., Brouwers, H.J.H., 2015. Characteristics and application potential of municipal solid waste incineration (MSWI) bottom ashes from two waste-to-energy plants. Constr. Build. Mater. 83, 77–94. https://doi.org/10.1016/j.conbuildmat.2015.02.033.

Tunell, G., Posnjak, E., Ksanda, C., 1935. Geometrical and optical properties and crystal structure of tenorite. Zeitschrift fur Krist. 90, 120–142.

Waychunas, G., Fuller, C., Davis, J., 2002. Surface complexation and precipitate geometry for aqueous Zn(II) sorption on ferrihydrite I: X-ray absorption extended fine structure spectroscopy analysis. Geochim. Cosmochim. Acta 66, 1119–1137. https://doi.org/10.1016/S0016-7037(01)00853-5.

Webb, S., 2005. Sixpack: A grapical user interface for XAS analysis using IFEFFIT. Phys. Scr., 1011–1014

Wei, Y., Shimaoka, T., Saffarzadeh, A., Takahashi, F., 2011. Mineralogical characterization of municipal solid waste incineration bottom ash with an emphasis on heavy metal-bearing phases. J. Hazard. Mater. 187, 534–543. https://doi.org/10.1016/j.jhazmat.2011.01.070.

Wyckoff, R., 1963. Crystal structures, volume 1.

Ziegler, F., Scheidegger, A.M., Johnson, C.A., Dähn, R., Wieland, E., 2001. Sorption Mechanisms of Zinc to Calcium Silicate Hydrate: X-ray Absorption Fine Structure (XAFS) Investigation. Env. Sci. Technol. 35, 1550–1555.